JOURNAL OF AIRCRAFT
Vol. 32, No. 3, May–June 1995

Analysis of Low Reynolds Number Airfoil Flows

J. A. Ekaterinaris,* M. S. Chandrasekhara,† and M. F. Platzer‡
Naval Postgraduate School, Monterey, California 93943-5100

Compressible steady and unsteady flowfields over a NACA 0012 airfoil at transitional Reynolds numbers are investigated. Comparisons with recently obtained experimental data are used to evaluate the ability of a numerical solution based on the compressible thin layer Navier–Stokes approximation, augmented with a transition model, to simulate transitional flow features. The discretization is obtained with an upwind-biased, factorized, iterative scheme. Transition onset is estimated using an empirical criterion based on the computed mean flow boundary-layer quantities. The transition length is computed from an empirical formula. The incorporation of transition modeling enables the prediction of the experimentally observed leading-edge separation bubbles. Results for steady airfoil flows at fixed angles of attack and for oscillating airfoils are presented.

Introduction

THE prediction of steady, inviscid flows over aerodynamic configurations is performed routinely nowadays. The computation of flows with separation bubbles or of fully separated flows, on the other hand, is still a very challenging problem. For many practical applications, the assumption of fully developed turbulent flow yields good predictions of the flowfield. In other circumstances, such as the leading-edge dynamic stall flow, this assumption is not valid and computations of such flows need improved methods.

A characteristic feature of the dynamic stall flow is the onset of compressibility effects at a very low freestream Mach number of 0.2.[1,2] In addition, at transitional Reynolds numbers, it has been shown[3,4] that the dynamic stall events are closely governed by the formation of a laminar separation bubble and its subsequent bursting. In fact, the above-cited studies demonstrate that the failure of the separated shear layer to reattach initiates dynamic stall, leading to the formation of the dynamic stall vortex. Further complications arise when the locally supersonic flow forms shocks that interact with the local boundary layer. It is important to recognize that the scales of the flow are very small here and the flow physics is not very clear. It is obvious that an accurate computational study of the problem demands a proper modeling of the physics of the local compressible flow. In an effort to reach this eventual goal, it is necessary to include the transition physics that plays a key role in the dynamic stall process. The study to be reported represents a step in this direction.

It is well known that prediction of the transition point and the transition length in such strongly adverse pressure gradient driven flows with current methods is difficult and involves uncertainties. Although several methods are available, the engineering prediction of transition relies on empirical formulation for boundary-layer flows. Whereas these methods have been moderately successful in steady and subsonic flows, in unsteady, compressible, incipiently separating flows the challenges are formidable, and thus, much needs to be done.

One method of transition prediction uses empirical formulations with an intermittency function distribution to evaluate an effective eddy viscosity in the transitional region. Another popular method is the e^N method. This method is based on the small amplitude, locally parallel flow assumptions that enable normal mode decomposition. Computation of the normal modes and their growth rates gives a criterion for the transition location. The criterion is based on the observation that transition occurs when the amplification rate reaches a value of $e^9 \approx 8100$. The e^N method accounts for the linear stability characteristics of the flow, and pressure gradient or curvature effects enter through the computed mean flow. Again, an empirical method must be used to obtain an effective eddy viscosity for the transitional flow region.

A more promising procedure for the prediction of transition has been recently developed by Herbert and Bertolotti,[5] and is known as the parabolized stability equation (PSE) method. The PSE method showed good agreement with direct numerical simulation (DNS) results, and is currently used for research studies on transition as an alternative to DNS. The PSE method coupled with a Navier–Stokes solution can be used for transition predictions in realistic geometries and boundary conditions. This approach has the advantage of providing a complete description of the flow in the transitional region, and it does not require empirical formulations, unlike the other two methods.

It is the objective of this article to show that it is crucial to model the leading-edge transitional flow in order to obtain physically realistic solutions to flows over airfoils at transitional Reynolds numbers, which include leading-edge separation bubbles. In a previous investigation Walker et al.[6] have shown that the separation bubble occurring on a NACA 65-213 airfoil for incompressible flow and $Re_c = 0.24 \times 10^6$ could be computed successfully using the Chen–Thyson[7] transition model. This model gives the turbulent intermittency γ_{tr} as a function of the computed boundary-layer quantities and a constant $G_{\gamma_{tr}}$. In Ref. 6 the transition constant of the model $G_{\gamma_{tr}}$, had to be chosen in the range between 20–40 rather than $G_{\gamma_{tr}} = 1200$, as originally suggested for high Reynolds number flows. Physically, a low value of the transition constant forces transition to take place over a shorter distance than at a higher value. Recent experiments by Gostelow et al.,[8] on the effects of freestream turbulence and adverse pressure gradient on boundary-layer transition, support the observation that a change in pressure gradient from zero to even a modestly adverse level is accompanied by a severe reduction in transition length. Even though it is expected that the computed solutions are sensitive to the choice of the transition

Presented as Paper 94-0534 at the AIAA 32nd Aerospace Sciences Meeting and Exhibit, Reno, NV, Jan. 10–13, 1994; received April 5, 1994; revision received Oct. 15, 1994; accepted for publication Oct. 20, 1994.

*Research Associate Professor, Navy–NASA Joint Institute of Aeronautics, Department of Aeronautics and Astronautics. Senior Member AIAA.

†Associate Director and Research Associate Professor, Navy–NASA Joint Institute of Aeronautics, Department of Aeronautics and Astronautics. Associate Fellow AIAA.

‡Director and Professor, Navy–NASA Joint Institute of Aeronautics, Department of Aeronautics and Astronautics. Associate Fellow AIAA.

constant $G_{\gamma_{tr}}$, here the transition constant is evaluated from an empirical formula that was used before for steady flows in Ref. 9.

Numerical Implementation

Numerical Scheme

The thin-layer approximation of the compressible, Reynolds-averaged, Navier–Stokes equations for body-fitted coordinate system ξ, η is used. These equations are as follows:

$$\partial_t \hat{q} + \partial_\xi \hat{F} + \partial_\eta \hat{G} = Re^{-1}\partial_\eta \hat{S}$$

here, $\hat{q}$ is the conservative variable vector, $\hat{q} = (\rho, \rho u, \rho v, e)^T$, $\hat{F}$ and $\hat{G}$ are the inviscid flux vectors, and $\hat{S}$ represents the thin-layer approximation of the viscous terms in the normal direction. In the above equations all geometrical dimensions are normalized with the airfoil chord length c; the density ρ is normalized with the freestream density ρ_∞; the Cartesian velocity components u, v of the physical domain are normalized with the freestream speed of sound a_∞; and the pressure p is normalized with p_∞.

Computation of transitional flows requires accurate mean flow solutions. The traditional central difference schemes for the compressible, governing equations provide second-order accuracy in space. Therefore, the following third-order, upwind-biased, factorized, iterative, implicit numerical scheme was used here to compute the mean flow:

$$\begin{aligned}[I + h_\xi(\nabla_\xi^b \tilde{A}_{i,k}^+ + \Delta_\xi^f \tilde{A}_{i,k}^-)]^p \times [I + h_\eta(\nabla_\eta^b \tilde{B}_{i,k}^+ + \Delta_\eta^f \tilde{B}_{i,k}^- \\ - Re^{-1}\delta_\eta \tilde{M}_{i,k})]^p \times (\tilde{Q}_{i,k}^{p+1} - \tilde{Q}_{i,k}^p) = -[(\tilde{Q}_{i,k}^p - Q_{i,k}^n) \\ + h_\xi(\tilde{F}_{i+1/2,k}^p - \tilde{F}_{i-1/2,k}^p) + h_\eta(\tilde{G}_{i,k+1/2}^p - \hat{G}_{i,k-1/2}^p) \\ - Re^{-1}h_\eta(\hat{S}_{i,k+1/2}^p - \tilde{S}_{i,k-1/2}^p)]\end{aligned}$$

In this equation, $h_\xi = \Delta\tau/\Delta\xi$, etc., $\tilde{A}^\pm = (\partial\tilde{F}/\partial\tilde{Q})$, etc., are the flux Jacobian matrices, and Δ, ∇, δ are the forward, backward, and central difference operators, respectively. The quantities $\tilde{F}_{i+1/2,k}$, $\tilde{G}_{i,k+1/2}$, and $\tilde{S}_{i,k+1/2}$ are numerical fluxes.

Time accuracy of the implicit numerical solution is obtained by performing Newton iteration to convergence within each time step. The approximation to $\tilde{Q}^{n+1}$ at each subiteration is the quantity $\tilde{Q}^p$. The inviscid fluxes $\hat{F}$ and $\hat{G}$ are evaluated using Osher's[9] upwinding scheme.

The numerical fluxes for a third-order accurate upwind-biased scheme are given by

$$\begin{aligned}\hat{F}_{i+1/2,k} = \tilde{F}_{i+1/2,k} + \tfrac{1}{6}[\Delta F_{i-1/2,k}^+ + 2\Delta F_{i+1/2,k}^+] \\ - \tfrac{1}{6}[\Delta F_{i+3/2,k}^- + 2\Delta F_{i+1/2,k}^-] = \tilde{F}(Q_{i,k}, Q_{i+1,k}) \\ + \tfrac{1}{6}[\Delta F^+(Q_{i+1,k}, Q_{i,k}) + 2\Delta F^+(Q_{i,k}, Q_{i+1,k})] \\ - \tfrac{1}{6}[\Delta F^-(Q_{i,k}, Q_{i+1,k}) + 2\Delta F^-(Q_{i+1,k}, Q_{i,k})]\end{aligned}$$

here, $\tilde{F}$ is the first-order accurate numerical flux for Osher's scheme[9] given by

$$\tilde{F}_{i+1/2,k} = \frac{1}{2}\left[F_{i,k} + F_{i+1,k} - \int_{Q_i}^{Q_{i+1}} (F_q^+ - F_q^-)\, dQ\right]$$

where $F_q = F_q^+ + F_q^-$, $F_q^\pm = (\partial F/\partial Q)^\pm$, and $\Delta F^\pm$ are the corrections to obtain high-order accuracy. For the linearization of the left-hand side (LHS) terms, the flux Jacobian matrices A, B are evaluated by the Steger–Warming[10] flux-vector splitting. The linearization errors are reduced by subiteration to convergence. Typically, two subiterations are sufficient to drop the residuals two orders of magnitude during the Newton iteration process. Accurate steady-state solutions can be obtained even without subiteration. Two subiterations are used for the unsteady solutions. The viscous fluxes $S_{i,k+1/2}$ are computed with central differences.

Transition Modeling

For the Reynolds number of the experiment based on the chord $Re_c = 0.54 \times 10^6$, it is known that a transitional flow region exists at the leading edge. Experimental investigations have shown that the structure of the near-wall flow dramatically changes when the flow is tripped at the leading edge. The focal point of this article is to show that it is necessary to account for the laminar/transitional/turbulent flow behavior in order to obtain meaningful flowfield predictions. Therefore, the computation starts as laminar from the stagnation point until transition onset by the empirical Michel criterion is detected. Transition according to Michel's criterion initiates once the Reynolds number based on the boundary-layer momentum thickness Re_θ is greater than the quantity $T = 1.174(1.0 + 22{,}400/Re_x)Re_x^{0.46}$, where Re_x is the Reynolds number at the specific x location from the stagnation point. The turbulent intermittency in the transitional region is estimated with the Chen–Thyson[7] formula as follows:

$$\gamma_{tr}(x) = 1 - \exp\left[\left(-\frac{U^3}{\nu^2 G_{\gamma_{tr}}}\right) Re_{x_{tr}}^{-1.34}(x - x_{tr}) \int_{x_{tr}}^{x} \frac{dx}{U}\right]$$

the value of the intermittency, $\gamma_{tr}(x)$ for $x \le x_{tr}$ is zero, and downstream from the transition point increases exponentially to a maximum value of one, which corresponds to the fully turbulent region. The $G_{\gamma_{tr}}$ value can alter the slope of the $\gamma_{tr}(x)$ curve and determines the extent of the transitional region. Here the $G_{\gamma_{tr}}$ value is estimated from

$$G_{\gamma_{tr}} = 213[\log(Re_x) - 4.732]/3$$

An effective eddy viscosity for the transitional region is obtained by scaling the turbulent eddy viscosity computed from the mean flow by $\gamma_{tr}(x)$. The turbulent eddy viscosity is obtained using the Baldwin–Barth model. Therefore, instead of ν_{turb}, an effective eddy viscosity $\nu_{trans} = \gamma_{tr}(x)\nu_{turb}$ is used throughout. The limitation of the present algebraic transition model is that it takes into account only the local flow characteristics, and other effects such as curvature, upstream influence, and pressure gradient are included only through the computed mean flow. It is also independent of the freestream turbulence level and other flow disturbances. It requires the evaluation of boundary-layer quantities that may be ambiguous or difficult to determine accurately for massively separated flow cases. Moreover, the intermittency function has only streamwise one-dimensional dependency and the normal-to-wall effects enter through the turbulent eddy viscosity obtained by the turbulence model. From an implementation point of view, however, the present transition model is quite simple to use and it can be easily incorporated to present computational fluid dynamics (CFD) codes and it can be combined with any turbulence model.

Results and Discussion

Recently, detailed measurements over a NACA 0012, 3-in. chord length airfoil flow have been performed by Chandrasekhara et al.[3,4,11,12] in the NASA Ames Research Center Fluid Mechanics Laboratory (FML) Compressible Dynamic Stall Facility (CDSF). The measurements were obtained for steady flow at fixed angles of incidence and for oscillatory motion of the airfoil. Here, the oscillatory motion with $\alpha(t) = 10° + 2° \sin(\omega t)$ in a freestream Mach number of 0.3 will be analyzed. The reduced frequency defined as $k = \pi fc/U_\infty$ was 0.05. For this case, the maximum angle of attack was 12 deg, which was below the static stall angle of 12.4 deg. Laser Doppler velocimetry (LDV) data and point diffraction interferometry (PDI) images were obtained through the oscillation cycle. Some of the results have been discussed in Refs. 13 and 14. The key result was that a separation bubble formed near the airfoil leading edge and it underwent changes through

the oscillation cycle. During the upstroke, the bubble simply grew in size. During the downstroke, the bubble decreased in size initially. However, as the airfoil angle decreased further, at about an angle of attack of 11.5 deg (i.e., less than the static stall angle), the vorticity in the bubble suddenly coalesced and was shed. At about half-a-degree later, i.e., at $\alpha = 11$ deg, the flow re-established itself, as it settled down to the conditions dictated by the lower angle of attack. This behavior was seen both in the vorticity distributions obtained from the LDV velocity data, which showed that the peak vorticity level drops at $\alpha = 11.5$ deg before increasing again at lower angles, and also, in the interferograms, which clearly show the separated shear layer and its reattachment later in the cycle. It appears, therefore, that this behavior of the separation bubble was caused by differences in vorticity input into the flow during the upstroke and downstroke.

Computational Results and Comparison with Experiments

In this article Navier–Stokes computations are presented for flow over a NACA 0012 airfoil at the same experimental conditions ($Re_c = 5.4 \times 10^5$ and $M_\infty = 0.3$), where the airfoil is either held at a constant angle of attack, or is oscillating as $\alpha(t) = 10° + 2° \sin(\omega t)$. A 275 × 91 point grid is used for the numerical solution. Grid points are concentrated around the suction peak location of the leading edge to provide better resolution of the transitional flow region. A normal spacing of $dy = 0.00001$ for the second point from the airfoil surface is used. The same computational mesh is used for both steady-state and unsteady solutions.

Steady Flow Studies

Results are first presented for flow over the NACA 0012 airfoil at fixed angles of attack of 5 and 6 deg where the flow is fully attached. Comparisons with the surface pressure distributions obtained by the PDI measurements are shown in Figs. 1 and 2. In these figures, the computed 100 × C_f and $\gamma_{tr}(x)$ distributions obtained by the Chen–Thyson formula are also shown. The agreement between computation and experiment is satisfactory for this low angle of incidence, where the flowfield is fully attached. The comparison of the measured and computed surface pressure coefficients over the entire airfoil is shown in Fig. 2b. The overall agreement between computation and experiment is good. The pressure coefficients are obtained from the densities measured in the interferometry using isentropic flow equations, even in the airfoil boundary-layer region. Single realizations of the interferogram are used in the comparison. The agreement is very good considering that the differences seen between the experimental and computational results are in general within the uncertainty of the experiment. Typically, the uncertainty in the interferometry technique is one fringe. Depending upon

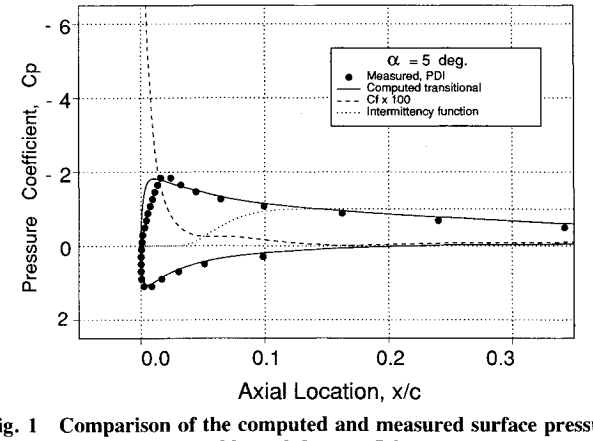

Fig. 1 Comparison of the computed and measured surface pressure coefficients; steady flow, $M_\infty = 0.3$, $\alpha = 5.0$ deg, $Re = 0.54 \times 10^6$.

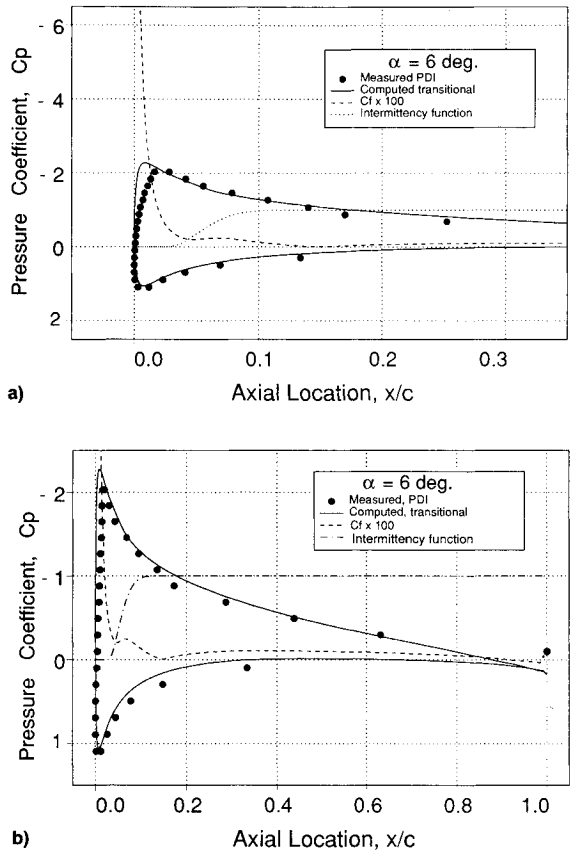

Fig. 2 Comparison of the computed and measured surface pressure coefficients; steady flow, $M_\infty = 0.3$, $\alpha = 6.0$ deg, $Re = 0.54 \times 10^6$.

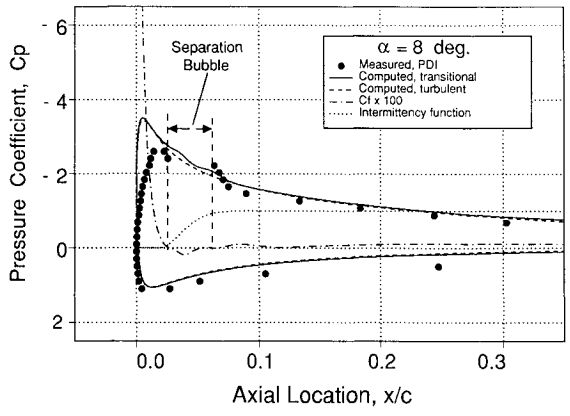

Fig. 3 Comparison of the computed and measured surface pressure coefficients; steady flow, $M_\infty = 0.3$, $\alpha = 8.0$ deg, $Re = 0.54 \times 10^6$.

the fringe number, this translates to an uncertainty level in C_p of up to about 0.20 per fringe (at low fringe numbers near the trailing edge for example). The x/c displacement seen at times is also within the range of fringe movement obtained in the experiment. Neither the experiment nor the computation indicate a bubble at $\alpha = 5$ and 6 deg.

In Figs. 3, 4, and 5, similar comparisons are shown for fixed angles of attack of 8, 10, and 12 deg. All three angles show the development of a separation bubble near the leading edge. The length of the separation bubble increases with increasing angle of attack. The γ_{tr} distributions plotted in these figures indicate the start of transition as predicted by the computation. The surface pressure coefficient obtained from a fully turbulent computation is also shown in Figs. 3, 4, and 5. For the lower angle of incidence ($\alpha = 8$ deg), the surface pressure coefficient obtained from a fully turbulent solution is close to

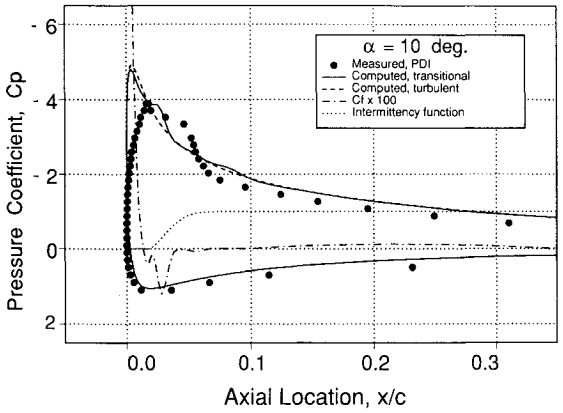

Fig. 4 Comparison of the computed and measured surface pressure coefficients; steady flow, $M_\infty = 0.3$, $\alpha = 10.0$ deg, $Re = 0.54 \times 10^6$.

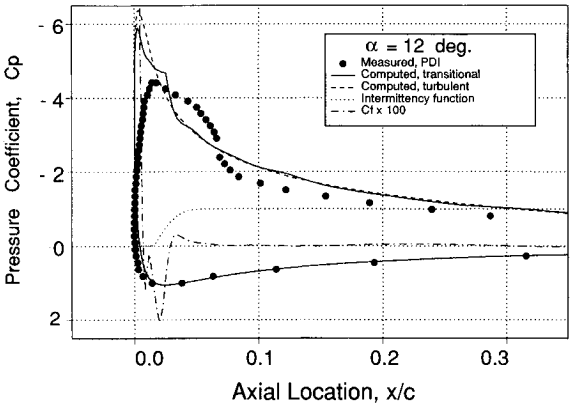

Fig. 5 Comparison of the computed and measured surface pressure coefficients; steady flow, $M_\infty = 0.3$, $\alpha = 12.0$ deg, $Re = 0.54 \times 10^6$.

that obtained by the transitional solution. However, there are significant differences (Fig. 3) between the measured and computed surface pressure distributions over most of the upper surface. The transition location onset predicted by the Michel criterion is upstream of the transition obtained in the experiment. As a result the computed separation bubble attains a smaller size. It should be noted that transition occurs somewhere in the plateau region of the measured pressure distribution, since the bubble forms originally from a separating laminar boundary layer (where the plateau begins). This shear layer undergoes transition slightly downstream and the resulting turbulence causes it to reattach further downstream (end of the bubble).

For $\alpha = 8.0$ deg, the transition onset by Michel criterion is obtained at $x/c = 0.015$. However, if the transition onset is specified at $x/c = 0.04$, which is the approximate location where transition initiates in the experiment, then a larger separation bubble is obtained. The agreement of the computed surface pressure coefficient with the experiment improves significantly when the transition onset is specified at $x/c = 0.04$. A systematic study on the sensitivity of the computed solution on the transition location has been carried out in Ref. 14.

For $\alpha = 8$ and 10 deg, the computed separation bubble forms in the transitional flow region, while for $\alpha = 12$ deg, the separation bubble begins in the laminar flow region and reattaches in the transitional flow region when compared to experiments. The discrepancies observed at 10 and 12 deg are similarly caused due to early initiation of transition as obtained by Michel criterion. The extent of the computed separation bubbles can be clearly discerned from the computed skin friction distributions. It is also seen that the measured

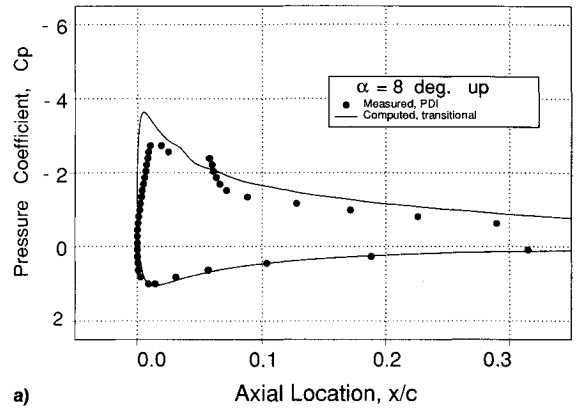

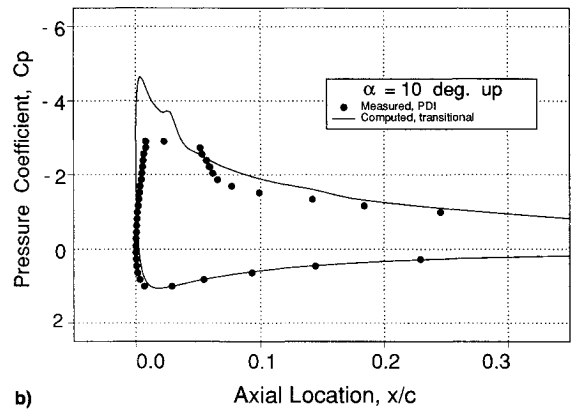

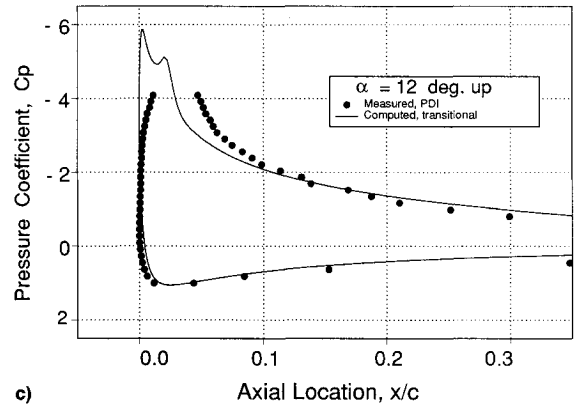

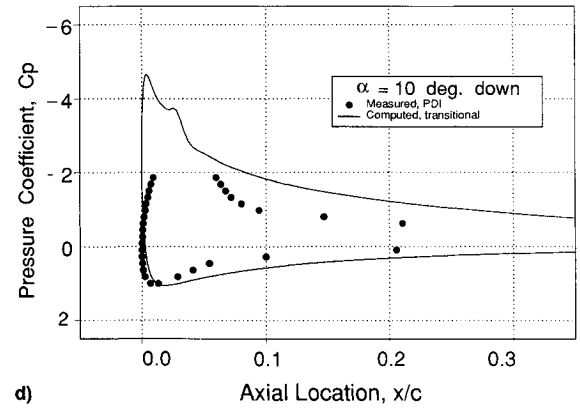

Fig. 6 Comparison of the computed and measured surface pressure coefficients; oscillatory flow a) $\alpha = 8.0$ deg, b) $\alpha = 10.0$ deg up, c) $\alpha = 12.0$ deg, and d) $\alpha = 10.0$ deg down; $M_\infty = 0.3$, $\alpha(t) = 10° + 2° \sin(\omega t)$, $k = 0.05$, $Re = 0.54 \times 10^6$.

bubbles are significantly longer than the computed ones. Interestingly, the fully turbulent solution fails to predict a separation bubble. This demonstrates that modeling of the transitional flow behavior is the key for capturing the major physical flow features.

The quantitative differences between the measured and computed bubbles are likely to be due to the deficiencies in modeling the transition. The Chen–Thyson model has no explicit dependence on adverse pressure gradient. However, recently in Ref. 8, Gostelow et al. have reported measurements on the effects of freestream turbulence and adverse pressure gradients on boundary-layer transition. These data need to be incorporated into the transition models and further systematic computations need to be made in order to achieve a better understanding of the complex physical mechanism of bubble formation. At $\alpha = 12$ deg, both the experiment and the computation showed some unsteadiness. Leading-edge separation has a significant effect on the overall development of the downstream turbulent flowfield, and significantly affects the unsteady flow results.

Oscillation $\alpha(t) = 10° + 2° \sin(\omega t)$

The unsteady solution was obtained with 20,000 time steps for the entire cycle, corresponding to a nondimensional time step of $\Delta t = 0.004$ or a Courant number of approximately 400. The solution progressed for three cycles and it was found that the solution for the third cycle coincided with the second cycle. The results presented here correspond to the second cycle. Comparisons with the experiment at four characteristic angles of incidence are conducted. The computed and measured surface pressure coefficients at the lowest angle of incidence during the oscillatory cycle $\alpha = 8$ deg are shown in Fig. 6a. The computed pressure coefficient shown on this figure indicates a small separation bubble which starts at $x/c = 0.025$ and ends at $x/c = 0.05$. At $\alpha = 10$ deg during the upstroke (Fig. 6b), the length of the separation bubble increases. At the peak of the oscillation cycle $\alpha = 12$ deg (Fig. 6c) the leading-edge separation bubble attains the largest size. Comparison of the computed and measured surface pressure coefficients during downstroke at $\alpha = 10$ deg also shows a leading-edge separation bubble. Again, as in the steady flow cases, significant differences between the computed and measured distributions are found. This is especially noticeable in Fig. 6d for the case of $\alpha = 10$ deg, on the downstroke. As mentioned earlier, the experiment showed that light stall occurred during the downstroke, which is caused by the shedding of the leading-edge vorticity. The computed separation bubbles were too small to cause shedding of the vortex. This may explain the large differences between the computation and the experiment shown in Fig. 6d.

Finally, the computed lift, drag, and pitching moment loops are shown in Figs. 7a–7c. Integrated loads are not available from the experiment. The figures show significant hysteresis effects that are not present in high Reynolds number flows and are not obtained by a fully turbulent computation.

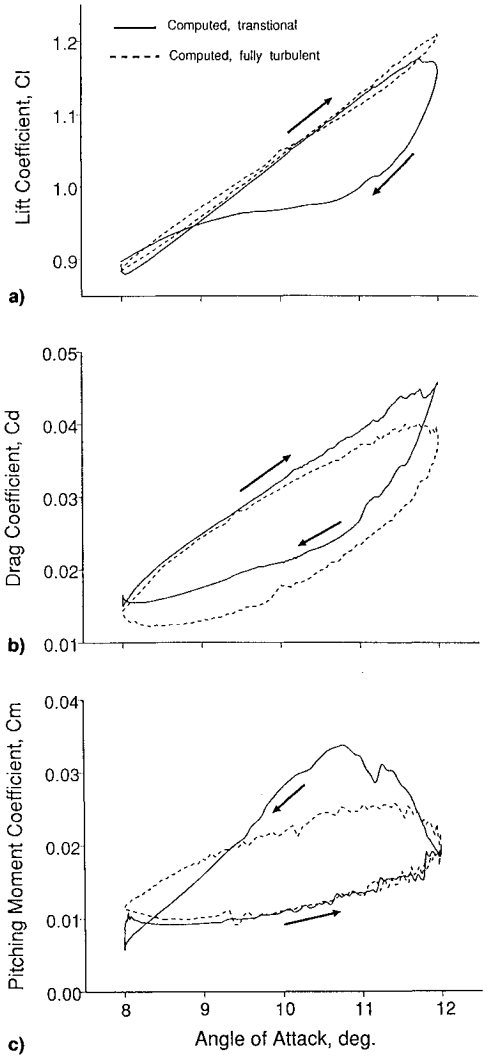

Fig. 7 Computed lift, drag, and pitching moment coefficients; oscillatory flow, $M_\infty = 0.3$, $\alpha(t) = 10° + 2° \sin(\omega t)$, $k = 0.05$, $Re = 0.54 \times 10^6$.

Conclusions

Numerical solutions for low Reynolds number flows over a NACA 0012 airfoil were obtained. It was found that it is crucial to model the leading-edge transitional flow behavior in order to obtain the experimentally observed separation bubbles. A simple empirical criterion was used for the prediction of the transition onset. The turbulent intermittency was obtained from an empirical formula based on the computed mean flow boundary-layer quantities.

Comparisons of the computed and PDI-derived pressure distributions show good agreement when no bubble is present. The inclusion of a transition model into the Reynolds-averaged Navier–Stokes equations is crucial to the successful prediction of leading-edge separation bubbles. The Chen–Thyson model used in this study should be improved using newly acquired data on the effect of adverse pressure gradient. Also, the dependency of the model on empirical constants should be reduced.

References

[1]McCroskey, W. J., "The Phenomenon of Dynamic Stall," NASA TM-81264, March 1981.

[2]Carr, L. W., "Progress in Analysis and Prediction of Dynamic Stall," *Journal of Aircraft*, Vol. 25, No. 1, 1988, pp. 6–17.

[3]Chandrasekhara, M. S., Carr, L. W., Ekaterinaris, J. A., and Platzer, M. F., "Interferometric and Computational Studies of an Oscillating Airfoil Compressible Dynamic Stall Flow Field," *Proceedings of the 5th Asian Congress of Fluid Mechanics*, Vol. 2, Taejon, Korea, 1992, pp. 1047–1050.

[4]Carr, L. W., Chandrasekhara, M. S., and Brock, N. J., "Quantitative Study of Unsteady Compressible Flow on an Oscillating Airfoil," *Journal of Aircraft*, Vol. 31, No. 4, 1994, pp. 892–898.

[5]Herbert, Th., and Bertolotti, F. P., "Stability Analysis of Nonparallel Boundary Layers," *Bulletin of the American Physical Society*, Vol. 32, Nov. 1987, p. 2079.

[6]Walker, G. J., Subroto, P. H., and Platzer, M. F., "Transition Modeling Effects on Viscous/Inviscid Interaction Analysis of Low Reynolds Number Airfoil Flows Involving Laminar Separation Bubbles," American Society of Mechanical Engineers Paper 88-GT-32, June 1988.

[7]Chen, K. K., and Thyson, N. A., "Extension of Emmons Spot Theory to Flows on Blunt Bodies," *AIAA Journal*, Vol. 9, No. 5, 1971, pp. 821–825.

[8]Gostelow, J. P., Blunden, A. R., and Walker, G. J., "Effects of Free-Stream Turbulence and Adverse Pressure Gradients on Boundary Layer Transition," American Society of Mechanical Engineers Paper 92-GT-380, June 1992.

[9]Jang, H. M., Ekaterinaris, J. A., Platzer, M. F., and Cebeci, T., "Essential Ingredients for the Computation of Steady and Unsteady Boundary Layers," *Journal of Turbomachinery*, Vol. 13, Oct. 1991, pp. 608–616.

[10]Osher, S., and Solomon, F., "Upwind Difference Schemes for Hyperbolic Systems of Conservation Laws," *Mathematics of Computation*, Vol. 38, No. 158, 1982, pp. 339–374.

[11]Steger, J. L., and Warming, R. F., "Flux Vector Splitting of the Inviscid Gas Dynamic Equations with Applications to Finite-Difference Methods," *Journal of Computational Physics*, Vol. 40, No. 2, 1981, pp. 263–293.

[12]Chandrasekhara, M. S., and VanDyken, R. D., "LDV Measurements in Dynamically Separated Flows," *Proceedings of the 5th International Conference on Laser Anemometry—Advances and Applications*, Vol. 2052, Society of Photo-Optical Instrumentation Engineers, 1993, pp. 305–312.

[13]VanDyken, R. D., and Chandrasekhara, M. S., "Leading Edge Velocity Field of an Oscillating Airfoil in Compressible Dynamic Stall," AIAA Paper 92-0193, Jan. 1992.

[14]VanDyken, R. D., Ekaterinaris, J. A., Chandrasekhara, M. S., and Platzer M. F., "Analysis of Transitional Reynolds Number Steady and Oscillatory Flows," AIAA Paper 94-2255, June 1994.